European Conference on Computational Fluid Dynamics
ECCOMAS CFD 2006
P. Wesseling, E. Oñate and J. Périaux (Eds)

AN OVERVIEW OF NUMERICAL METHODS FOR ACOUSTIC WAVE PROPAGATION

Christophe Bailly and Christophe Bogey

Laboratoire de Mécanique des Fluides et d'Acoustique,
Ecole Centrale de Lyon & UMR CNRS 5509
36 avenue Guy de Collongue, 69134 Ecully cedex, France
e-mail: christophe.bailly@ec-lyon.fr
web page: http://acoustique.ec-lyon.fr/

Key words: finite-difference schemes, dispersion relation, acoustic propagation, Euler's equations, computational aeroacoustics

Abstract. *This paper presents a short overview of recent developments of low-dispersive and low-dissipation finite-difference schemes as an alternative to more classical methods of applied mathematics. Needs of accurate and efficient numerical solvers in computational aeroacoustics have motivated these developements over the last two decades. Properties of the differencing methods are illustrated through theoretical analyses and numerical experiments.*

1 INTRODUCTION

Computational AeroAcoustics is focused on the direct computation of aerodynamic noise, namely the unsteady turbulent field and the radiated noise by this flow. Accurate numerical algorithms are required to achieve this goal, and have been developped over the last twenty years.[1] Most of them are concerned with space and time finite-difference schemes, and the present paper is a brief survey of these numerical methods.

The paper is structured as follows. As a starting point, equations governing linear acoustic propagation in an inhomogeneous moving medium are recalled in § 2. Model problems used in numerics for investigating long-range acoustic propagation are also given. Space discretization based on finite-differences are presented in § 3, and explicit optimized Runge-Kutta algorithms are discussed in § 4.

2 WAVE EQUATIONS

Acoustics is usually considered as a linear problem governed by the compressible linearized Euler equations[2,3] in order to describe mean flow effects on sound propagation, such as refraction. It is for instance well known that the high-frequency noise radiated by a source inside a jet is diverting away from the jet axis, and that a shadow zone is

observed at angles close to the jet axis.[4] The linearized Euler equations can be written as

$$\begin{cases} \partial_t \rho' + \boldsymbol{u}_0.\nabla\rho' + \boldsymbol{u}'.\nabla\rho_0 + \rho_0\nabla.\boldsymbol{u}' = 0 \\ \rho_0\left(\partial_t \boldsymbol{u}' + \boldsymbol{u}_0.\nabla\boldsymbol{u}' + \boldsymbol{u}'.\nabla\boldsymbol{u}_0\right) + \nabla p' - (\rho'/\rho_0)\nabla p_0 = 0 \\ \partial_t s' + \boldsymbol{u}_0.\nabla s' + \boldsymbol{u}'.\nabla s_0 = 0 \end{cases} \tag{1}$$

where ρ is the density, $\boldsymbol{u}$ the velocity, p the pressure and s the entropy. The mean flow variables are denoted by a subscript 0, and the perturbated field by a prime '. For a perfect gas, the linearization of the equation of state can take the form

$$p' = c_0^2\rho' + (p_0/c_v)s'$$

where c_v is the specific heat at constant volume and $c \equiv \partial p/\partial\rho|_s$ is the speed of sound. In a more general case, as for underwater acoustics for instance, the system (1) is closed by the relation

$$\partial_t p' + \boldsymbol{u}_0.\nabla p' + \boldsymbol{u}'.\nabla p_0 = c_0^2\left(\partial_t\rho' + \boldsymbol{u}_0.\nabla\rho' + \boldsymbol{u}'.\nabla\rho_0\right) + (c^2)'\boldsymbol{u}_0.\nabla\rho_0$$

Note that in a medium at rest ($\boldsymbol{u}_0 = 0$), the term ∇p_0 in (1) is simply the hydrostatic pressure, in equilibrium with the force of gravity, and is generally neglected[5] for frequencies $f \gg 10^{-3}$ Hz.

Many efforts have been developed to obtain approached solutions by using geometrical acoustics[6] or parabolic approximations.[7] They are still the only techniques available to solve practical propagation problems in complex environments, such as in underwater acoustics or in a turbulent atmosphere,[8] even if *ad-hoc* assumptions are necessarily introduced to obtain efficient numerical algorithms.

Numerical developments are also based on model problems for long-range acoustic propagation. The one-dimensional advection equation can be thus considered as a archetype for numerical studies. The equation to be solved is

$$\partial_t u + c\partial_x u = 0 \tag{2}$$

where c is a constant. The initial perturbation $u(x,0) = g(x)$ simply propagates at the speed c, and the solution is given by $u(x,t) = g(x-ct)$. Competition between nonlinear convection and diffusion can be also investigated by considering the one-dimensional Burger equation,[9]

$$\partial_t u + u\partial_x u = (4/3)\mu\partial_{xx} u \tag{3}$$

where μ is the dynamical viscosity. Nonlinear effects can be finally studied through the one-dimensional Euler equation,

$$\frac{\partial \boldsymbol{U}}{\partial t} + \frac{\partial \mathbf{E}}{\partial x} = 0 \qquad \boldsymbol{U} = \begin{pmatrix} \rho \\ \rho u \\ \rho e_t \end{pmatrix} \qquad \mathbf{E} = \begin{pmatrix} \rho u \\ \rho u^2 + p \\ (\rho e_t + p)u \end{pmatrix} \tag{4}$$

where ρe_t is the total energy $\rho e_t = p/(\gamma - 1) + \rho u^2/2$ and γ the ratio of the specific heats.

In addition, note that insightful problems are available in the proceedings of the four workshops on benchmark problems in computational aeroacoustics.[10–13]

3 FINITE DIFFERENCES FOR SPATIAL DERIVATIVES

3.1 Explicit finite-difference schemes

Let us consider a one-dimensional uniform mesh of spacing Δx. An explicit finite-difference approximation of the spatial derivative $\partial_x u$ at grid point $x = l\Delta x$ is given by

$$\left.\frac{\partial u}{\partial x}\right|_l \simeq \frac{1}{\Delta x} \sum_{j=-M}^{N} a_j u_{l+j} \tag{5}$$

for a $(M + N + 1)$-point stencil. This relation is a particular case of the more general continuous relation

$$\frac{\partial u}{\partial x} \simeq \frac{1}{\Delta x} \sum_{j=-M}^{N} a_j u(x + j\Delta x) \tag{6}$$

and the discrete relation (5) is recovered by setting $x = x_l$ in (6). This modeling introduces numerical dissipation and dispersion, namely errors in the amplitude and in the propagation speed of the waves respectively. To show that, the approximation of the exact wavenumber k can be derived by taking the Fourier transform of (6),

$$ik\hat{u} \simeq \frac{\hat{u}}{\Delta x} \sum_{j=-M}^{N} a_j e^{ijk\Delta x}$$

where $\hat{u}(k)$ is the Fourier transform of $u(x)$ defined by

$$u(x) = \int_{-\infty}^{+\infty} \hat{u}(k) e^{ikx} dk \tag{7}$$

The effective, or intrinsic or modified, wavenumber k_s of the finite difference can be thus defined as

$$k_s \Delta x \equiv -i \sum_{j=-M}^{N} a_j e^{ijk\Delta x} = 2 \sum_{j=1}^{N} a_j \sin(jk\Delta x) \tag{8}$$

by choosing antisymmetric coefficients, $a_j = -a_{-j}$ for $j = 1, \ldots, N$. A centered scheme ensures indeed a real wavenumber and allows to remove any dissipation error. The numerical dispersion relation (8) is plotted in figure 1 for different standard central schemes, where the coefficients a_j are determined to cancel the Taylor series of (6) so that the maximum order is reached, in $\mathcal{O}(\Delta x^{2N})$ for a $(2N + 1)$-point scheme. These coefficients

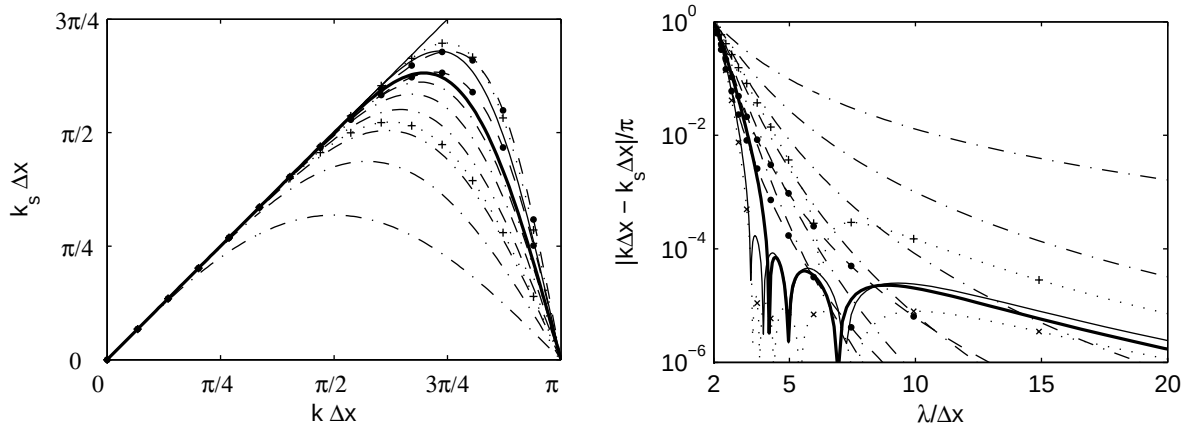

Figure 1: Effective wavenumber (8) as a function of the exact wavenumber for spatial differencing methods: left, linear representation and right, logarithmic scales. −·−·− 2nd, 4th, 6th, 8th 10th and 12th-order central differences, ···+··· DRP 7-point scheme of Tam and Webb[14] and ···×··· DRP 15-point scheme,[13] −●− tridiagonal 6th-order compact 5-point scheme ($\alpha = 1/3$) and 8th-order ($\alpha = 3/8$) scheme of Lele,[20] optimized ——— 11-point and —— 13-point schemes of Bogey and Bailly.[15]

satisfy the following N equations

$$2\sum_{j=1}^{N} a_j j^q = \delta_{1,2q-1} \quad \text{for} \quad q = 1, \ldots, N \tag{9}$$

Optimized schemes can also be obtained by minimizing the error on the modified wavenumber, which can be defined as the integral error[14]

$$\int_{k_l\Delta x}^{k_u\Delta x} |k_s\Delta x - k\Delta x|^2 \, d(k\Delta x)$$

over a large wavenumber range $k_l \leq k \leq k_u$, or also by minimizing the relative error[15]

$$\int_{k_l\Delta x}^{k_u\Delta x} \frac{|k_s\Delta x - k\Delta x|}{k\Delta x} \, d(k\Delta x) = \int_{\ln(k_l\Delta x)}^{\ln(k_u\Delta x)} |k_s\Delta x - k\Delta x| \, d\ln(k\Delta x)$$

For instance, the optimized 11-point scheme of Bogey & Bailly[15] is of 4th-order, and the last three conditions in (9) are replaced by the minimization of the integral relative error over $k_l = \pi/16 \leq k \leq k_u = \pi/2$.

The modified wavenumber of some classical central schemes[14,15] used in computational aeroacoustics are reported in figure 1. Spectral-like resolution can be obtained with optimized schemes. Note also that perturbations at the highest wavenumber $k\Delta x = \pi$ corresponding to the odd-even mode are never resolved according to the Nyquist-Shannon theorem.

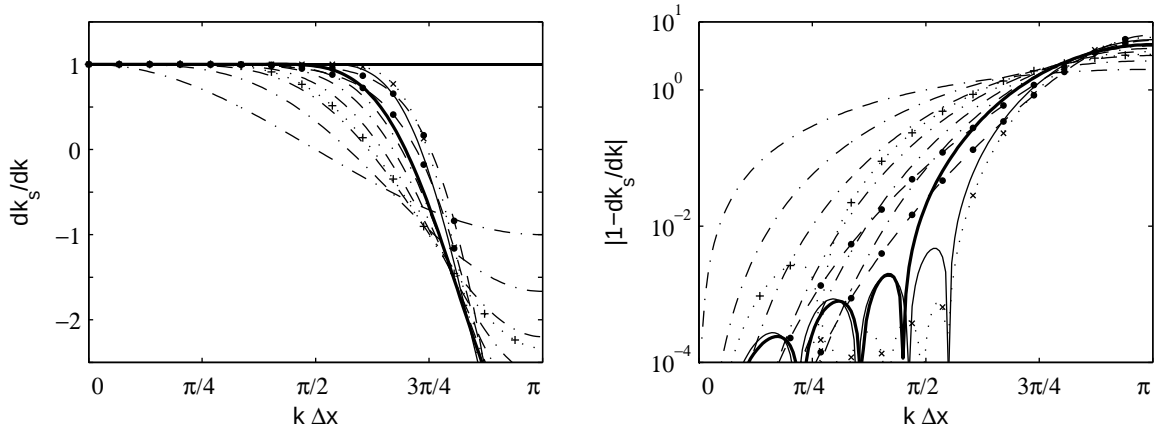

Figure 2: Group velocity as a function of the exact wavenumber for spatial differencing methods: left, linear representation and right, logarithmic scale. –·–·– 2nd, 4th, 6th, 8th 10th and 12th-order central differences, $\cdots+\cdots$ DRP 7-point scheme of Tam and Webb[14] and $\cdots\times\cdots$ DRP 15-point scheme,[13] $-\bullet-$ tridiagonal 6th-order compact 5-point scheme ($\alpha = 1/3$) and 8th-order ($\alpha = 3/8$) scheme of Lele,[20] optimized ━━ 11-point and —— 13-point schemes of Bogey and Bailly.[15]

The error curves $k_s = k_s(k)$ presented in figure 1 correspond to the numerical dispersion introduced by the semi-discrete approximation (6), and observed for a simple-harmonic plane wave $e^{i(kx-\omega t)}$ propagating at the phase speed $v_\varphi = \omega/k = ck_s/k$ by solving the advection equation (2) for instance. For a non-harmonic problem however, the crests of the waves still propagate at the phase velocity but the energy of the wave-packet moves at the group velocity

$$v_g = \frac{\partial \omega}{\partial k} = c\frac{\partial k_s}{\partial k}$$

The evolution of an initial wave-packet $u(x, t = 0) = g(x)$ is indeed given by

$$u(x,t) = \int_{-\infty}^{+\infty} \hat{g}(k) e^{i(kx-\omega t)} dk \tag{10}$$

for $t \geq 0$, where $\hat{g}(k)$ is the Fourier transform (7) of the initial perturbation. An asymptotic solution can be derived by the theorem of the stationary phase[16–18] as $t \to \infty$ along a given ray $x/t = \text{cte}$. By introducing the phase function $\phi(k) = kx/t - \omega$, the cancellation is obtained where $\phi'(k^\star) = 0$, *i.e.*

$$\frac{\partial \omega}{\partial k} = \frac{x}{t}$$

For each wavenumber $k^\star$, the integral (10) can thus take the form

$$u(x,t) \sim \sqrt{2\pi/t/\omega''(k^\star)}\, \hat{g}(k)\, e^{i(k^\star x - \omega t) + i\frac{\pi}{4}\mathrm{sgn}[\omega''(k^\star)]} \tag{11}$$

along the path $x = v_g(k^\star)\, t$ as $t \to \infty$, with $\omega''(k^\star) = \partial^2\omega/\partial k^2|_{k^\star} \neq 0$. As expected, the component of the wave packet associated with the wavenumber $k^\star$ propagates at the

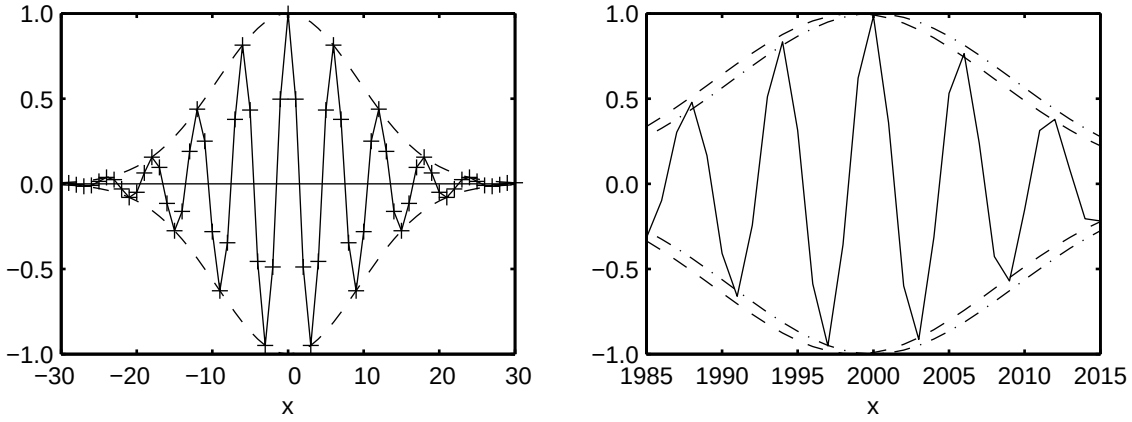

Figure 3: Propagation of a wave-packet. Left, —— initial perturbation (12) and – – – its envelope. Right, numerical solution obtained at time $t = 2000$ with the optimized 11-point scheme.[15] The two envelopes obtained with the group velocity – – – $e^{-\ln 2\,[(x-v_g t)/b]^2}$, and with the phase velocity –·–·– $e^{-\ln 2\,[(x-v_\varphi t)/b]^2}$, are also plotted for comparison.

group speed $v_g(k^\star)$. By solving this problem with the semi-discrete approximation (6), the numerical dispersion will be thus imposed by the error on the group velocity $v_g = c\partial k_s/\partial k$ of the finite-difference scheme. It is straightforward to obtain its expression from (8),

$$\frac{\partial k_s}{\partial k} = 2\Delta x \sum_{m=0}^{\infty} \sum_{j=1}^{N} j a_j \frac{(jk\Delta x)^{2m}}{(2m)!}$$

and to note that for a centered finite-difference scheme of order $2N$, the leading behaviour of the group velocity is $v_g = \mathcal{O}(\Delta x^N)$ as $k\Delta x \to 0$. Figure 2 displays the curves $\partial k_s/\partial k$ of the differencing schemes considered in figure 1. The error on the group velocity is larger than that on the phase velocity, but the relative accuracy of the different schemes is similar.

As an exemple of the use of the group velocity, consider the advection equation (2) of the initial wavetrain

$$g(x) = e^{-\ln 2\,(x/b)^2}\ \cos(k_w x) \tag{12}$$

with the values $b/\Delta x = 11$ and $k_w \Delta x = \pi/3$, which corresponds to an oscillatory part with 6 points per wavelength. The initial perturbation is shown in figure 3, and the spatial derivative is performed with the optimized 11-point scheme.[15] The propagation equation is integrated with an optimized 4th-order Runge-Kutta scheme[19] and a small time step Δt in order to only evaluate features of the spatial scheme. For simplicity, the test problem is solved on a uniform grid $\Delta x = 1$, with a velocity $c = 1$ and the CFL number is taken to be $\beta = c\Delta t/\Delta x = 0.2$. The numerical solution obtained at time $t = 2000$ is also reported in figure 3. As expected, the wave packet propagates at the group velocity $v_g = v_g(k_w) \simeq 0.9994$, and is thus centered at $x = v_g \times t \simeq 1998.80$, as shown in the figure, rather than at $x = v_\varphi \times t \simeq 1999.80$.

scheme	$E_{v_\varphi} \leq 5 \times 10^{-5}$			$E_{v_g} \leq 5 \times 10^{-4}$	
	$k\Delta x\|_{\max}$	$\lambda/\Delta x\|_{\min}$	$k_m\Delta x$	$k\Delta x\|_{\max}$	$\lambda/\Delta x\|_{\min}$
CFD 2nd-order	0.0986	63.7	1.0000	0.0323	194.6
CFD 4th-order	0.3439	18.3	1.3722	0.2348	26.8
CFD 6th-order	0.5857	10.7	1.5860	0.4687	13.4
CFD 8th-order	0.7882	8.0	1.7306	0.6704	9.4
CFD 10th-order	0.9550	6.6	1.8374	0.8380	7.5
CFD 12th-order	1.0929	5.7	1.9208	0.9768	6.4
DRP 7-pts 4th-order	0.4810	13.1	1.6442	0.3500	18.0
DRP 15-pts 4th-order	1.8069	3.5	2.1914	1.6070	3.9
FDo 11-pts 4th-order	1.3530	4.6	1.9836	0.8458	7.4
FDo 13-pts 4th-order	1.3486	4.7	2.1354	0.7978	7.9
CoFD 6th-order	0.8432	7.5	1.9894	0.7201	8.7
CoFD 8th-order	1.1077	5.7	2.1334	0.9855	6.4

Table 1: Accuracy limits of some explicit central finite-difference schemes. CFD designes standard central finite-difference schemes, DRP is the Dispersion-Relation-Preserving scheme of Tam & Webb,[14] FDo are the optimized schemes of Bogey & Bailly[15] and CoFD is the tridiagonal compact scheme of Lele[20] for $\alpha = 1/3$ (6th-order) and $\alpha = 3/8$ (8th-order). The error criteria on phase and group velocities are defined by $E_{v_\varphi} = |k_s\Delta x - k\Delta x|/\pi \leq 5 \times 10^{-5}$ and $E_{v_g} = |\partial k_s/\partial k - 1| \leq 5 \times 10^{-4}$ respectively. Accuracy limits are equally provided in terms of point-per-wavelength resolution ($\lambda/\Delta x$), and the highest modified wavenumber $k_m\Delta x$ corresponding to a zero group velocity is also given.

Table 1 summarizes accuracy limits based on both phase- and group-velocity errors, obtained by using the arbitrary criteria $E_{v_\varphi} = |k_s\Delta x - k\Delta x|/\pi \leq 5 \times 10^{-5}$ and $E_{v_g} = |\partial k_s/\partial k - 1| \leq 5 \times 10^{-4}$. As mentioned before, the error on the group velocity is larger by construction. The optimized 11-point scheme appears as a good compromise between accuracy and numerical efficiency.

3.2 Implicit finite-difference schemes

Implicit formulations based on a Pade-type development[20,22] can also be used to compute the approximation of the space derivative at point x_l

$$\alpha \left.\frac{\partial u}{\partial x}\right|_{l-1} + \left.\frac{\partial u}{\partial x}\right|_{l} + \alpha \left.\frac{\partial u}{\partial x}\right|_{l+1} = a\frac{u_{l+1} - u_{l-1}}{2\Delta x} + b\frac{u_{l+2} - u_{l-2}}{4\Delta x} + c\frac{u_{l+3} - u_{l-3}}{6\Delta x}$$

A α-family of 6th-order tridiagonal schemes is obtained with the relations $a = (\alpha+9)/6$, $b = (32\alpha - 9)/15$ and $c = (-3\alpha + 1)/10$ on the coefficients. Two particular values are of interest, $\alpha = 1/3$ leading to a compact 5-point stencil and, $\alpha = 3/8$, allowing to reach the 8th-order. Furthermore, the standard explicit scheme is retrieved as $\alpha \to 0$. The modified wavenumber can be found by Fourier analysis

$$k_s\Delta x = \frac{a\sin(k\Delta x) + (b/2)\sin(2k\Delta x) + (c/3)\sin(3k\Delta x)}{1 + 2\alpha\cos(k\Delta x)}$$

and is reported in figures 1 and 2. A good resolution is reached, as shown more quantitatively in table 1.

3.3 Selective spatial filtering

It must be observed that the highest wavenumbers, unresolved by finite-difference schemes, must be removed by a selective filtering in order to preserve the long waves accurately discretized. An artificial numerical damping is thus introducing in the continuous model $\mathcal{L}(u) = 0$, and takes the general form of a convolution product

$$\mathcal{L}(u) = -(\sigma_d/\Delta t)(1 - G) * u$$

where σ_d specifies the strength of the filtering, $0 \leq \sigma_d \leq 1$. The corresponding discretized equation may be written as

$$u_l^f = u_l - \sigma_d \sum_{j=-N}^{N} d_j u_{l+j}$$

The coefficients d_j of the discrete filter are such as $d_{-j} = d_j$ to ensure no dispersion, and must verify two conditions of normalization and realizability. In addition, it is often required that the first kth moments of G are zero,[21] and the coefficients can also be optimized in the Fourier space.[15] The transfer function $G_k = 2\pi\hat{G}$ of the filter reads

$$G_k = 1 - d_0 - 2\sum_{j=1}^{N} d_j \cos(jk\Delta x)$$

and is usually plotted for some explicit filtering in figure 4. In pratical applications, the filtering is applied at every time iteration with a value $\sigma_d \leq 0.2$ and the condition $|\sigma_d\,(1 - G_k)| \leq 5 \times 10^{-5}$ can be used to define the range of long waves not appreciably affected by filter. Table 2 gives this wavenumber limit for some standards and optimized explicit filters. For a 11-point stencil, which represents a good compromise between accuracy and numerical efficiency for the spatial derivative, the optimized 11-point filter provides better results for resolved short waves whereas the 10th-order standard filter has a lower dissipation for long waves. The performance of the optimized filter is indeed limited by its low formal order.

As for spatial schemes, implicit selective filters have been proposed and used by Lele,[20] and Gaitonde & Visbal[22,23] among others. For a tridiagonal formulation, the filtered value u_l^f is obtained by solving the system

$$\alpha_f u_{l-1}^f + u_l^f + \alpha_f u_{l+1}^f = \sum_{j=0}^{N} \frac{a_j}{2}(u_{l+j} + u_{l-j})$$

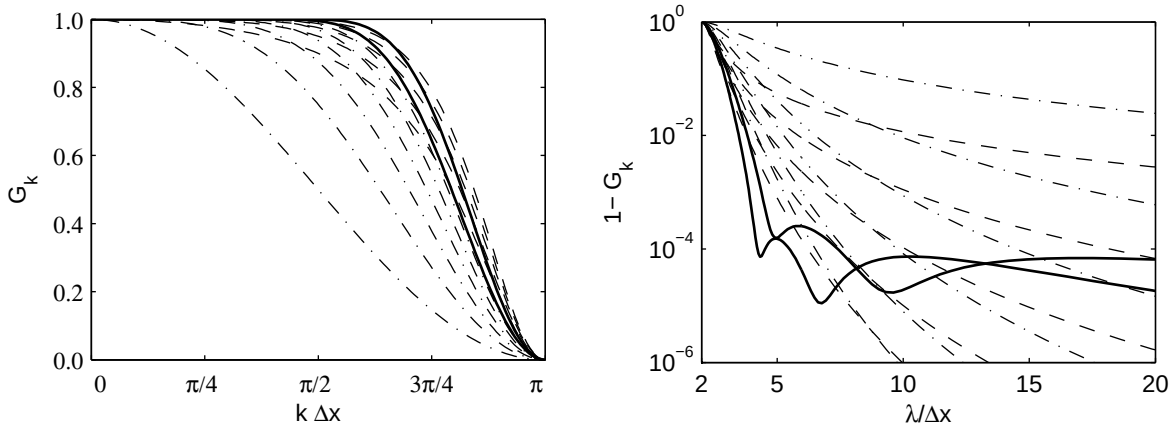

Figure 4: Transfer function $G_k(k\Delta x)$ of some explicit filters: left, linear representation and right, logarithmic scale. −·−·− 2nd, 4th, 6th, 8th, 10th and 12th-order standard filters, − − − tridiagonal 2nd, 4th, 6th, 8th and 10th-order implicit filters[20,22] with $\alpha_f = 0.4$, —— optimized 11-point 2nd-order and 13-point 4th-order selective filters of Bogey and Bailly.[15]

explicit	$\lvert\sigma_d\,(1-G_k)\rvert \leq 5\times10^{-5}$		implicit	$\lvert 1-G_k\rvert \leq 5\times10^{-5}$	
filters	$k\Delta x\rvert_{\max}$	$\lambda/\Delta x\rvert_{\min}$	filters	$k\Delta x\rvert_{\max}$	$\lambda/\Delta x\rvert_{\min}$
2nd-order	0.0323	194.5	2nd-order	0.0428	146.9
4th-order	0.2523	24.9	4th-order	0.2915	21.6
6th-order	0.5080	12.4	6th-order	0.5552	11.3
8th-order	0.7254	8.7	8th-order	0.7688	8.2
10th-order	0.9035	7.0	10th-order	0.9419	6.7
12th-order	1.0501	6.0			
Opt. 11-pts 2nd-order	1.0475	6.0			
Opt. 13-pts 4th-order	1.5407	4.1			

Table 2: Accuracy limits of some filters, with $\sigma_d = 0.2$ for explicit filters and $\alpha_f = 0.4$ for the tridiagonal implicit filters.[20,22]

where α_f must be such as $-0.5 < \alpha_f < 0.5$, and lie in the interval $0.3 \leq \alpha_f < 0.5$ in practice.[22,23] The corresponding transfer function reads

$$G_k(k\Delta x) = \frac{\sum_{j=0}^{N} a_j \cos(jk\Delta x)}{1 + 2\alpha_f \cos(k\Delta x)}$$

and is reported in figure 4 and table 2. Accuracy is in agreement with the formal order of the filter, and the corresponding explicit standard filtering is recovered as $\alpha_f \to 0$.

3.4 Concluding remarks

All the scales supported by a grid are not well resolved by a finite-difference scheme. Accuracy can be measured directly from the spatial derivative by a Fourier analysis. Minimizing the error on the effective wavenumber is equivalent to control the phase-velocity error k_s/k which is relevant for a simple harmonic plane wave. The group-velocity error $\partial k_s/\partial k$ is also involved for the propagation of a wavetrain as $t \to \infty$. Magnitude of the group velocity error is higher by construction but both errors are strongly linked as shown by the accuracy limits given in table 1, which allows to define well-resolved wavenumbers $0 \leq k \leq k_c^s$. The unresolved wavenumbers $k_c^s \leq k \leq k_c^g = \pi/\Delta$ must be removed by a filtering operation by leaving unaffected the long physical waves and with a cutoff frequency $k_c^f \leq k_c^s$. This point is important for applications in order to control the stability for grid-to-grid oscillations, or to avoid configurations such as $v_g.v_\varphi < 0$ when Perfectly Matched Layer (PML) techniques are used for instance.[24]

The extension of all these schemes to 3-D Cartesian grids is straightforward but many other points needs to be discussed, such as near-boundary schemes,[23,25] the use of non uniform meshes,[15] curvilinear meshes,[22,26] and the treatment of boundary conditions.[27]

4 TIME INTEGRATION

The numerical features of time integration can be also studied and optimized in a similar way. Time schemes fall into one of the two following classes of algorithm: Adams-Bashford or multi-step methods, and Runge-Kutta or multi-stage methods. A review can be found in Butcher,[28] and only explicit Runge-Kutta schemes are discussed hereafter.

4.1 Explicit Runge-Kutta schemes

Consider now the semi-discrete differential equation

$$\frac{\partial u^n}{\partial t} = F(u^n, t)$$

where $u^n(x) = u(x, n\Delta t)$. The general form of an explicit Runge-Kutta scheme at p-stages reads

$$u^{n+1} = u^n + \Delta t \sum_{i=1}^{p} b_i K^i \quad \text{with} \quad K^i = F\left(u^n + \sum_{j=1}^{i-1} a_{ij} K^j, t^n + c_i \Delta t\right) \tag{13}$$

where the coefficients c_i are given by $c_i = \sum_{j=1}^{i-1} a_{ij}$ for $i = 1, \ldots, p$. For instance, the standard 4th-order Runge-Kutta scheme with $p = 4$ stages is obtained with the following coefficients

c_i	a_{ij}
	b_i

$c_1 = 0$	0			
$c_2 = 1/2$	1/2			
$c_3 = 1/2$	0	1/2		
$c_4 = 1$	0	0	1	
	1/6	1/3	1/3	1/6

The formal order of the scheme (13) is derived by matching the coefficients with the Taylor series of $u(t^n + \Delta t)$. As an illustration, the following relations are deduced for the 4th-order scheme after a tedious calculation

$$\begin{array}{llll} (c1)\ \sum b_i = 1 & (c2)\ \sum b_i c_i = \frac{1}{2} & (c3)\ \sum b_i c_i^2 = \frac{1}{3} & (c3)\ \sum b_i a_{ij} c_j = \frac{1}{6} \\ (c4)\ \sum b_i c_i^3 = \frac{1}{4} & (c4)\ \sum b_i c_i a_{ij} c_j = \frac{1}{8} & (c4)\ \sum b_i a_{ij} c_j^2 = \frac{1}{12} & (c4)\ \sum b_i a_{ij} a_{jk} c_k = \frac{1}{24} \end{array}$$

where (ck) denotes the condition which must be satisfied to obtain the kth-order.[28,29] Several formulations have been proposed to reduce storage requirements[19,30–32] and to improve accuracy.[15,33,34] For exemple, Williamson[30] imposes $b_p = 1$ and $b_i = 0$ for $i = 1, \ldots, p-1$. Only the coefficients $a_{i\,i-1}$ are non-zero, and the time-marching algorithm (13) can be reduce to

$$u^{n+1} = u^n + \alpha_p \Delta t K^p \quad \text{with} \quad K^i = F\left(u^n + \alpha_{i-1} K^{i-1}, t^n + c_i \Delta t\right) \tag{14}$$

with only two storages per grid point for each variable.

From the time Fourier transform defined as

$$u(t) = \int_{-\infty}^{+\infty} \hat{u}(\omega) e^{-i\omega t} d\omega$$

an amplification factor $R_s = \hat{u}^{n+1}/\hat{u}^n$ can be introduced and calculated from (13). The integration error is then estimated by comparison between the exact amplification factor $R_e = e^{-i\omega\Delta t}$ and the effective amplification factor of the scheme, which takes the form

$$R_s = 1 + \sum_{j=1}^{p} \gamma_j (-i\omega\Delta t)^j \tag{15}$$

Stability requires an amplification rate such as $|R_s(\omega\Delta t)| < 1$, and integration errors can be measured by comparing $R_s = |R_s| e^{-i\omega_s \Delta t}$ with the exact amplification factor R_e, in terms of dissipation error with $1 - |R_s|$, and of phase error with $|\omega_s \Delta t - \omega\Delta t|/\pi$. These errors are shown in figures 5 and 6 for some schemes used in aeroacoustics. All the schemes considered have interesting properties, but the logarithmic representation of the amplitude and phase errors on the amplification rate demonstrate the good behaviour of the low-storage optimized 4th-order Runge-Kutta scheme derived by Berland[19] *et al.*

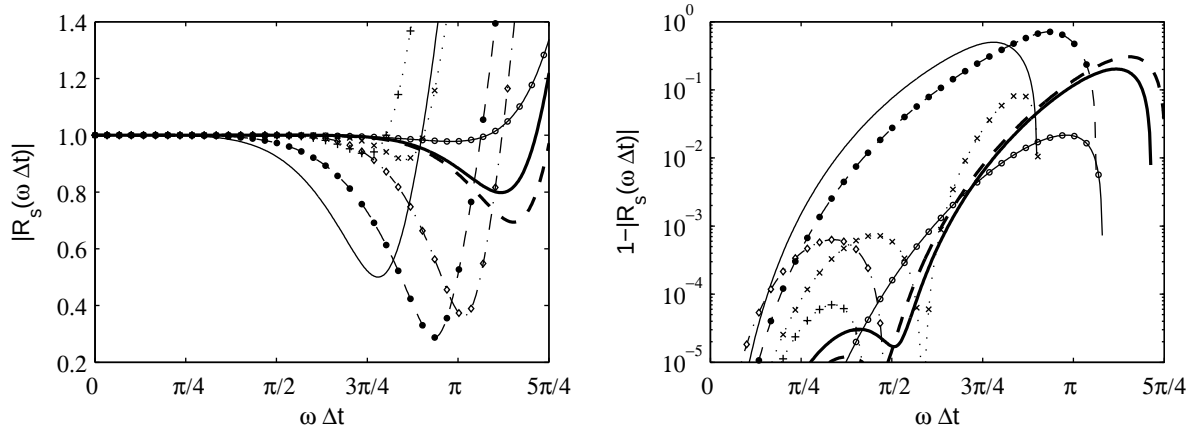

Figure 5: Modulus of the amplification factor (15) as a function of the angular frequency: left, linear representation and right, logarithmic scale. —— standard 4th-order RK, —○— standard 8th-order RK, ···+··· LDDRK46 Hu,[34] ···×··· LDDRK56 Hu,[34] —●— 4th-order 2N-RK Carpenter,[33] —·◇—· opt. 4th-order 2N Stanescu,[31] - - - opt. 2nd-order RK Bogey,[15] ——— opt. 4th-order 2N-RK Berland.[19]

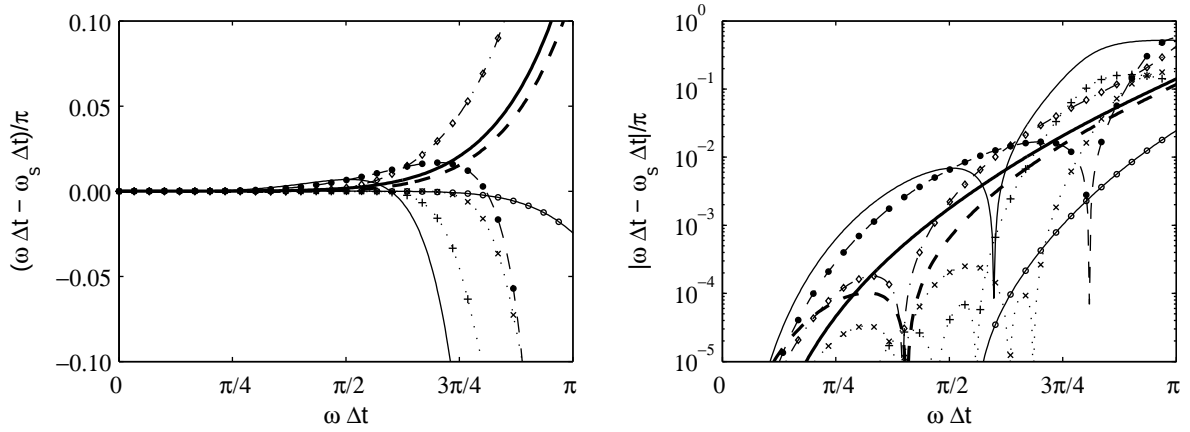

Figure 6: Phase error as a function of the angular frequency: left, linear representation and right, logarithmic scale. —— standard 4th-order RK, —○— standard 8th-order RK, ···+··· LDDRK46 Hu,[34] ···×··· LDDRK56 Hu,[34] —●— 4th-order 2N-RK Carpenter,[33] —·◇—· opt. 4th-order 2N Stanescu,[31] - - - opt. 2nd-order RK Bogey,[15] ——— opt. 4th-order 2N-RK Berland.[19]

scheme	formal order	$E_d \leq 5 \times 10^{-4}$		$E_\varphi \leq 5 \times 10^{-4}$		stability	
		$\omega\Delta t\|_{\max}$	β	$\omega\Delta t\|_{\max}$	β	$ck_m\Delta t\|_{\max}$	β
Standard RK4	4th	0.65	0.33	0.75	0.38	2.83	1.42
Standard RK8[29]	8th	1.79	0.90	2.23	1.12	3.39	1.71
Stanescu[31]	4th	0.87	0.44	1.39	0.70	1.51	0.76
Carpenter[33]	4th	0.80	0.40	0.88	0.45	3.34	1.68
Opt. LDDRK46[34]	4th	1.58	0.80	1.87	0.94	1.35	0.68
Opt. LDDRK56[34]	4th	1.18	0.59	2.23	1.13	2.84	1.43
Opt. 2N-RK Bogey[15]	2nd	1.91	0.96	1.53	0.77	3.94	1.99
Opt. 2N-RK Berland[19]	4th	1.97	0.99	1.25	0.63	3.82	1.92

Table 3: Accuracy limits of some explicit Runge-Kutta schemes. The CFL number limit $\beta = c\Delta t/\Delta x$ is given for the optimized 11-point finite difference scheme as illustration.[15]

Two arbitrary criteria are used to estimate quantitatively the accuracy of the different schemes, $E_d = 1 - |R_s(\omega\Delta t)| \leq 5 \times 10^{-4}$ and $E_\varphi = |\omega\Delta t - \omega_s\Delta t|/\pi \leq 5 \times 10^{-4}$. The values are reported in table 3, and are also expressed with a Courant condition. Stability, for instance, is obtained by a constraint on the angular frequency $\omega\Delta t \leq A$. Using the dispersion relation of the advection equation (2), this condition takes the form $ck_s\Delta t \leq A$ or $\beta \leq A/(k_s\Delta x)$ where the CFL number is defined by $\beta = c\Delta t/\Delta x$. The stability limit is thus obtained by taking the maximum effective wavenumber $k_m\Delta x$, provided in table 1. Forhe different time schemes studied in table 3, the two optimized schemes developed by Bogey[15] *et al.* and Berland[19] *et al.* are definitely among the most accurate, with a large time-step range of stability.

4.2 Numerical Dispersion relation

To carry on the discussion starting in § 3.1, the numerical group velocity which governs the propagation of a wavetrain must now include the dispersion arising from the time integration. A suitable combination has to be used for the space and the time derivative to minimize the error on this numerical group velocity.

5 CONCLUSION

Some key ideas for the derivation of accurate finite-difference algorithms have been discussed in this paper. Many other points and methods have to be considered to provide a complete overview of the topic. Practical details for the implementation of these techniques can be found in applications dealing with the direct computation of noise.

REFERENCES

[1] T. Colonius and S. Lele, "Computational aeroacoustics: progress on nonlinear problems on sound generation", *Progress in Aerospace Sciences*, **40**, 345–416 (2004).

[2] D. Blokhintzev, "The propagation of sound in an inhomogeneous and moving medium I", *J. Acoust. Soc. Am.*, **18**(2), 322–328 (1946).

[3] M.E. Goldstein, *Aeroacoustics*, McGraw-Hill, New York (1976).

[4] J. Atvars, L.K. Schubert and H.S. Ribner, "Refraction of sound from a point source placed in an air jet", *J. Acoust. Soc. Am.*, **37**, 168–170 (1965).

[5] R.R. Goodman and R.W. Farwell, "A note on the derivation of the wave equation in an inhomogeneous ocean", *J. Acoust. Soc. Am.*, **66**(6), 1895–1896 (1979).

[6] S.M. Candel, "Numerical solution of conservation equations arising in linear wave theory: application to aeroacoustics", *J. Fluid Mech.*, **83**(3), 465–493 (1977).

[7] F.B. Jensen and C.M. Ferla, "Numerical solutions of range-dependent benchmark problems on ocean acoustics", *J. Acoust. Soc. Am.*, **87**(4), 1499–1510 (1990).

[8] P. Chevret, P. Blanc-Benon and D. Juvé, "A numerical model for sound propagation through a turbulent atmosphere near the ground", *J. Acous. Soc. Am.*, **100**(6), 3587–3599 (1996).

[9] E.R. Benton and G.W. Platzman, "A table of solution of the one-dimensional Burgers equation", *Quart. Appl. Math.*, **30**, 195–212 (1972).

[10] "Workshop on benchmark problems in computational aeroacoustics", edited by J.C. Hardin, J.R. Ristorcelli and C.K.W. Tam, *NASA*, CP - 3300 (1995).

[11] "Second computational aeroacoustics workshop on benchmark problems", edited by C.K.W. Tam and J.C. Hardin, *NASA*, CP - 3352 (1997).

[12] "Third computational aeroacoustics (CAA) workshop on benchmark problems", edited by M.D. Dahl, *NASA*, CP - 2000-209790 (2000).

[13] "Fourth computational aeroacoustics (CAA) workshop on benchmark problems", edited by M.D. Dahl, *NASA*, CP - 2004-212954 (2003).

[14] C.K.W. Tam, C.K.W. and J.C. Webb, "Dispersion-relation-preserving finite difference schemes for computational acoustics", *J. Comput. Phys.*, **107**, 262–281 (1993).

[15] C. Bogey and C. Bailly, "A family of low dispersive and low dissipative explicit schemes for noise computation", *J. Comput. Phys.*, **194**(1), 194–214, (2004).

[16] G.B. Whitham, *Linear and nonlinear waves*, John Wiley & Sons, New York (1999).

[17] J. Lighthill, *Waves in fluids*, Cambridge University Press, Cambridge (1978).

[18] L.N. Trefethen, "Group velocity in finite difference schemes", *SIAM Review*, **24**(2), 113–136 (1982).

[19] J. Berland, C. Bogey and C. Bailly, "Low-dissipation and low-dispersion fourth-order Runge-Kutta algorithm", *Comput. & Fluids*, available on-line, 1–5 (2006).

[20] S.K. Lele, "Compact finite difference schemes with spectral-like resolution", *J. Comput. Physics*, **103**(1), 16–42 (1992)

[21] O.V. Vasilyev, T.S. Lund and P. Moin, "A general class of commutative filters for LES in complex geometries", *J. Comput. Phys.*, **146**, 82–104 (1998).

[22] M.R. Visbal and D.V. Gaitonde, "Very high-order spatially implicit schemes for computational acoustics on curvilinear meshes", *J. Comput. Acoust.*, **9**(4), 1259–1286 (2001).

[23] D.V. Gaitonde and M.R. Visbal, "Padé-type higer-order boundary filters for the Navier-Stokes equations", *AIAA Journal*, **38**(11), 2103–2112 (2000).

[24] F.Q. Hu, "A perfectly matched layer absorbing boundary condition for linearized Euler equations with a non-uniform mean flow", *J. Comput. Phys.*, **208**, 469–492 (2005).

[25] J. Berland, C., Bogey and C. Bailly, "Optimized explicit schemes: matching and boundary schemes, and 4th- order Runge-Kutta algorithm", *10th AIAA/CEAS Aeroacoustics Conference*, May 10-12, Manchester (U.K.), AIAA Paper 2004-2814 (2004).

[26] O. Marsden, C., Bogey and C. Bailly, "High-order curvilinear simulations of flows around non-Cartesian bodies", *J. Comput. Acoust.*, **13**(4), 731–748 (2005).

[27] T. Colonius, "Modeling artificial boundary conditions for compressible flows", *Annu. Rev. Fluid Mech.*, **36**, 315–345 (2004).

[28] J.C. Butcher, "Numerical methods for ordinary differential equations in the 20th century", *Journal of Computational and Applied Mathematics*, **125**, 1–29 (2000).

[29] J.R. Dormand and P.J. Prince, "A family of embedded Runge-Kutta formulae", *J. of Computational and Applied Maths.*, **6**(1), 19–26 (1980).

[30] J.H. Williamson, "Low-storage Runge-Kutta schemes", *J. Comput. Phys.*, **35**, 48–56 (1980).

[31] D. Stanescu and W.G. Habashi, "2N-storage Runge-Kutta schemes for acoustics", *J. Comput. Phys.*, **143**, 674–681 (1998).

[32] M. Calvo, J.M. Franco and L. Rández, "A new minimum storage Runge-Kutta scheme for computational acoustics", *J. Comput. Phys.*, **201**, 1–12 (2004).

[33] M.H. Carpenter and C.A. Kennedy, "Fourth-order, 2N-storage Runge-Kutta schemes", *NASA* TM 109112 (1994).

[34] F.Q. Hu, M.Y. Hussaini and J.L. Manthey, "Low-dissipation and low-dispersion Runge-Kutta schemes for computational acoustics", *J. Comput. Phys.*, **124**, 177–191 (1996).